Available online at www.sciencedirect.com
SCIENCE DIRECT®
Journal of Sound and Vibration 263 (2003) 797–813
JOURNAL OF SOUND AND VIBRATION
www.elsevier.com/locate/jsvi

Determination of flutter derivatives via a neural network approach

C.H. Chen*

Department of Civil Engineering, Chung Yuan Christian University, 22 Pu-Jen, Pu-chung Li, Chungli 32023, Taiwan, ROC

Received 30 November 2001; accepted 3 September 2002

Abstract

A neural-network-based method is offered to determine the flutter derivatives of section models under smooth and turbulent flows. The approach uses the observed dynamic responses to train an appropriate neural network. Subsequently, the modal parameters of the model for different mean velocities of wind flow are directly estimated using weight matrices in the neural network. The flutter derivatives can then be determined accurately. The validity of the present method is verified through numerical studies. Finally, the procedure is employed to process experimental data from an inverted-U-type section model, obtained from wind tunnel tests.
© 2002 Elsevier Science Ltd. All rights reserved.

1. Introduction

Flutter derivatives are aeroelastic parameters and are crucial to the aeroelastic stability analysis of cable-supported bridges. Accordingly, the determination of the flutter derivatives has stimulated the interest of many researchers. Based on experimental results, Scanlan and Tomko [1] first proposed eight flutter derivatives to represent the self-excited forces caused by wind. The authors also utilized the logarithmic decrement parameter for damping to determine some flutter derivatives by considering free oscillation data measured by three different experiments. However, Kumarasena [2] stated that the procedure of Scanlan and Tomko [1] cannot determine easily all the flutter derivatives. Advanced system identification techniques have also been used to establish the flutter derivatives from the results of typical wind tunnel tests that involved torsional and vertical responses under various flow conditions (for example, smooth and turbulent flow).

*Corresponding author. Tel.: +886-3-2654220; fax: +886-3-2654299.
E-mail address: chernhwa@cycu.edu.tw (C.H. Chen).

0022-460X/03/$ - see front matter © 2002 Elsevier Science Ltd. All rights reserved.
doi:10.1016/S0022-460X(02)01279-8

Shinozuku et al. [3] used the auto-regressive and moving-average (ARMA) model, cooperating with the instrumental variable (IV) method and limited information maximum likelihood (LIML) method, to determine the flutter derivatives of a 2-D suspension bridge model, from the dynamic responses caused by the self-excited and buffeting forces. Imai et al. [4] reviewed and compared some system identification methods for processing structural dynamic responses: he considered the ordinary least-squares (OLS) method, IV method, maximum likelihood (ML) method and extended Kalman filter. These researchers concluded that the IV and ML methods performed better than OLS method in estimating the structural parameters for a 2-D suspension bridge model. Sakar et al. [5,6] developed the modified ITD (MITD) by introducing instrumental variables into ITD. Theoretically, the MITD method can only process free vibration signals; therefore, this method is not expected to handle effectively the dynamic responses to buffeting forces unless the buffeting forces are a broadband spectrum. Poulsen et al. [7] used the stochastic realization identification method to estimate the eight flutter derivatives from dynamic responses that included vertical and torsional modes, while Yamada et al. [8] and Iwamoto and Fujino [9] used the extended Kalman filter, combined with the autoregressive (AR) model. Bogunovic Jakobsen and Hjorth-Hansen [10] proposed the covariance block Hankel matrix method to estimate flutter derivatives from buffeting response data.

Over the previous two decades, artificial neural networks (ANN) have gradually become known as powerful tools in pattern recognition, signal processing, control, and complex mapping, because of their excellent capacity for learning and high tolerance to partially inaccurate data [11]. This paper aims to show how flutter derivatives can be estimated using ANN to process the dynamic responses of a bridge deck coming from both the self-excited and the buffeting forces. Conventional back-propagation is employed to train ANN by using the aeroelastic responses of a section model. A procedure is developed to estimate directly the dynamic characteristics of the section model based on the weighting matrices of the trained ANN. The flutter derivatives are then determined from the identified dynamic characteristics. Numerically simulated aeroelastic responses of a bridge deck to the self-excited and buffeting forces are examined to confirm the validity of the proposed procedure. Finally, the procedure is applied to process the responses measured in typical wind tunnel tests.

2. Governing equations for an aerodynamic system

For an idealized 2-D aerodynamically coupled section model, as shown in Fig. 1, the equations of motion under turbulent flow can be written as

$$\begin{bmatrix} \bar{m} & 0 \\ 0 & \bar{I} \end{bmatrix} \begin{Bmatrix} \ddot{h} \\ \ddot{\alpha} \end{Bmatrix} + \begin{bmatrix} c_{11} & c_{12} \\ c_{21} & c_{22} \end{bmatrix} \begin{Bmatrix} \dot{h} \\ \dot{\alpha} \end{Bmatrix} + \begin{bmatrix} k_{11} & k_{12} \\ k_{21} & k_{22} \end{bmatrix} \begin{Bmatrix} h \\ \alpha \end{Bmatrix} = \begin{Bmatrix} L_{se} \\ M_{se} \end{Bmatrix} + \begin{Bmatrix} L_b \\ M_b \end{Bmatrix}, \tag{1}$$

where h is the vertical displacement, α is the torsional angle, $\bar{m}$ is the mass, $\bar{I}$ is the mass moment of inertia, and c_{ij} and k_{ij} are the mechanical damping and stiffness coefficients between degrees of freedom, i and j, respectively. L_{se} and M_{se} are, respectively, the self-excited forces corresponding to h and α, induced by the mean wind velocity, while L_b and M_b are the buffeting forces associated with h and α, due to turbulent wind.

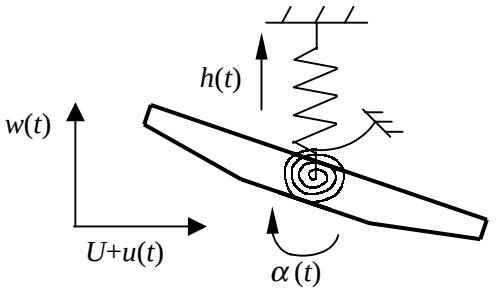

Fig. 1. A typical layout of a 2-D section model in wind tunnel test.

In a smooth wind flow, with mean velocity U, L_{se} and M_{se} are idealized as [12]

$$L_{se} = \frac{1}{2}\rho U^2 B\left[KH_1^*\left(\frac{\dot{h}}{U}\right) + KH_2^*\left(\frac{\dot{\alpha}}{U}\right) + K^2 H_3^*\alpha + K^2 H_4^*\left(\frac{h}{B}\right)\right], \tag{2}$$

$$M_{se} = \frac{1}{2}\rho U^2 B^2\left[KA_1^*\left(\frac{\dot{h}}{U}\right) + KA_2^* B\left(\frac{\dot{\alpha}}{U}\right) + K^2 A_3^*\alpha + K^2 A_4^*\left(\frac{h}{B}\right)\right], \tag{3}$$

where ρ is the air density, B is the deck width, and H_i^* and A_i^* are non-dimensional flutter derivatives. The flutter derivatives are functions of the reduced frequency, K ($= B\omega_s/U$, where ω_s is the frequency of the system). The buffeting forces corresponding to h and α are given as [13]

$$L_b = \frac{1}{2}\rho U^2 B\left[C_L\left(\frac{2u(t)}{U}\right) + \left(\frac{\partial C_L}{\partial\alpha} + C_D\right)\left(\frac{w(t)}{U}\right)\right], \tag{4}$$

$$M_b = \frac{1}{2}\rho U^2 B^2\left[C_M\left(\frac{2u(t)}{U}\right) + \frac{\partial C_M}{\partial\alpha}\left(\frac{w(t)}{U}\right)\right], \tag{5}$$

where C_L, C_D, and C_M are the static lift, and drag and moment coefficients, respectively, and are functions of the wind's angle of attack, α, $u(t)$ and $w(t)$ are the along-wind and vertical velocity fluctuations of the wind, respectively.

Substituting Eqs. (2) and (3) into Eq. (1), and rearranging, yields

$$\mathbf{M}\begin{Bmatrix}\ddot{h}\\ \ddot{\alpha}\end{Bmatrix} + \mathbf{C}^{eff}\begin{Bmatrix}\dot{h}\\ \dot{\alpha}\end{Bmatrix} + \mathbf{K}^{eff}\begin{Bmatrix}h\\ \alpha\end{Bmatrix} = \begin{Bmatrix}L_b\\ M_b\end{Bmatrix}, \tag{6}$$

where

$$\mathbf{M} = \begin{bmatrix}\bar{m} & 0\\ 0 & \bar{I}\end{bmatrix},$$

$$\mathbf{C}^{eff} = \begin{bmatrix}c_{11}^{eff} & c_{12}^{eff}\\ c_{21}^{eff} & c_{22}^{eff}\end{bmatrix},$$

$$\mathbf{K}^{eff} = \begin{bmatrix}k_{11}^{eff} & k_{12}^{eff}\\ k_{21}^{eff} & k_{22}^{eff}\end{bmatrix}.$$

c_{ij}^{eff} and k_{ij}^{eff} are called the effective damping and stiffness coefficients between degrees of freedom, i and j, at a mean wind velocity U, respectively, and are given as

$$\begin{aligned} c_{11}^{eff} &= c_{11} - \tfrac{1}{2}\rho UBKH_1^*, & k_{11}^{eff} &= k_{11} - \tfrac{1}{2}\rho U^2K^2H_4^*, \\ c_{12}^{eff} &= c_{12} - \tfrac{1}{2}\rho UB^2KH_2^*, & k_{12}^{eff} &= k_{12} - \tfrac{1}{2}\rho U^2BK^2H_3^*, \\ c_{21}^{eff} &= c_{21} - \tfrac{1}{2}\rho UB^2KA_1^*, & k_{21}^{eff} &= k_{21} - \tfrac{1}{2}\rho U^2BK^2A_4^*, \\ c_{22}^{eff} &= c_{22} - \tfrac{1}{2}\rho UB^3KA_2^*, & k_{22}^{eff} &= k_{22} - \tfrac{1}{2}\rho U^2B^2K^2A_3^*. \end{aligned} \tag{7}$$

Notably, C^{eff} and K^{eff} are commonly not symmetric. Moreover, C^{eff} is no longer a proportional damping matrix.

3. Backpropagation identification network

An artificial neural network model is a system with inputs and outputs that is based on biological nerves. The system can consist of many computational elements that operate in parallel and are arranged in patterns that resemble biological neural nets. A neural network is usually characterized by its computational elements, its network topology, and the learning algorithm employed. Among the several types of ANN, the feedforward, multilayered, supervised neural network with the error backpropagation algorithm—the backpropagation network (BPN) [14] is by far the most popular neural network learning model, because of its simplicity.

The architecture of BP networks, shown in Fig. 2, includes an input layer, one or more hidden layers and an output layer. Every node in each layer is connected to every node in the adjacent layer. Notably, Hecht-Nielsen [15] demonstrated that one hidden layer of neurons suffices to model any solution surface of practical interest. Hence, this study addresses a network with only one hidden layer. Before an ANN can be used, it must be trained using an existing training set of pairs of input–output elements.

The training of a supervised neural network using a BP learning algorithm typically proceeds in three stages. The first stage is the data feedforward. The computed output of the ith node in the output layer is defined as follows:

$$y_i = g\left(\sum_{j=1}^{N_h}\left(w_{ij}g\left(\sum_{k=1}^{N_i} v_{jk}x_k + \theta_{vj}\right) + \theta_{wi}\right)\right), \quad i = 1, 2, \ldots, N_o, \tag{8}$$

where w_{ij} is the connective weight between nodes in the hidden layer and those in the output layer, v_{jk} is the connective weight between nodes in the input layer and those in the hidden layer, θ_{wi} (or θ_{vj}) are bias terms that represent the threshold of the transfer function g, and x_k is the input of the kth node in the input layer. Terms N_i, N_h, and N_o are the numbers of nodes in the input, hidden, and output layers, respectively. The transfer function can be linear or non-linear. This work used a linear transfer function, defined as

$$g(q) = q. \tag{9}$$

The second stage is error backpropagation through the network. During training, a system error function monitors the performance of the network. This function is commonly defined

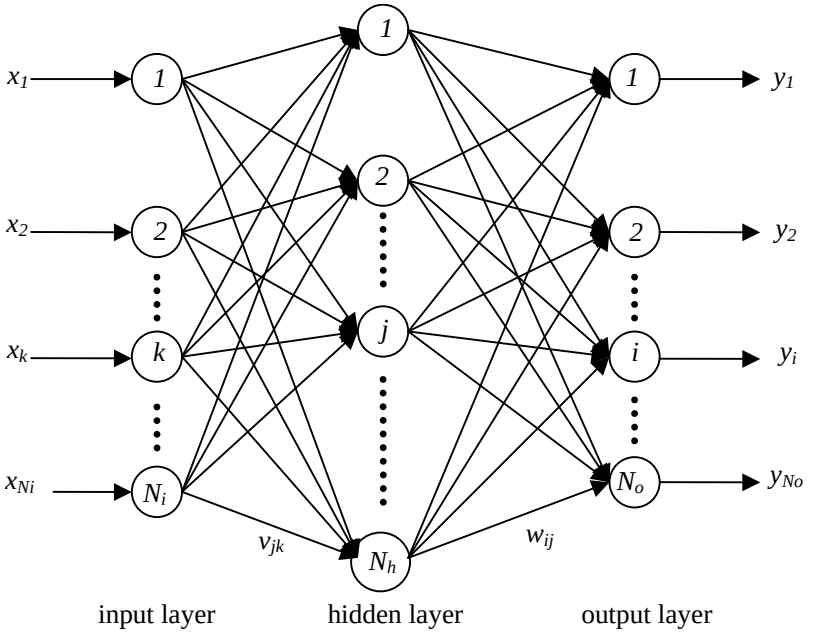

Fig. 2. A typical three-layer neural network.

as follows:

$$E(s) = \frac{1}{2P}\sum_{p=1}^{P}(\tilde{\mathbf{Y}}_p - \mathbf{Y}_p)(\tilde{\mathbf{Y}}_p - \mathbf{Y}_p)^{\mathrm{T}}, \tag{10}$$

where $\tilde{\mathbf{Y}} = (\tilde{y}_1\tilde{y}_2\cdots\tilde{y}_i\cdots\tilde{y}_{N_o})$, $\mathbf{Y} = (y_1y_2\cdots y_i\cdots y_{N_o})$, $\tilde{y}_i$ is the desired (or measured) value of output node i, p is the total number of data points for each input node, and $s = (v_{11}v_{12}\cdots v_{jk}\cdots v_{N_hN_i}\theta_{v1}\theta_{v2}\cdots\theta_{vN_h}w_{11}w_{12}\cdots w_{ij}\cdots w_{N_oN_h}\theta_{w1}\theta_{w2}\cdots\theta_{wN_o})$, the vector of parameters to be determined in a ANN.

The final stage is the adjustment of the weights. For computational efficiency, the Marquardt–Levenberg algorithm [16] is applied to obtain w_{ij}, v_{jk}, θ_{wi} and θ_{vj} by minimizing $E(s)$ in Eq. (10).

4. Identification of flutter derivatives

Obtaining the responses, $h(t)$ and $\alpha(t)$, and the inputs, $u(t)$ and $w(t)$, in Eq. (6) from a numerical simulation or, experimentally, from wind tunnel tests with smooth flow, enables a neural network to be constructed, as depicted in Fig. 3, to predict $h(t)$ and $\alpha(t)$ from previous responses, $h(t-i)$ and $\alpha(t-i)$, and inputs $u(t-j)$ and $w(t-j)$, where $i = 1, 2, 3, \ldots, n$, $j = 0, 1, 2, \ldots, m$. Variables n and m represent the lags in the output and input, respectively. Eqs. (8) and (9) can be combined to show easily that the neural network in Fig. 3 can be mathematically described as

$$\{Y\} = [W][V]\{X\} + ([W]\{\theta_v\} + \{\theta_w\}), \tag{11}$$

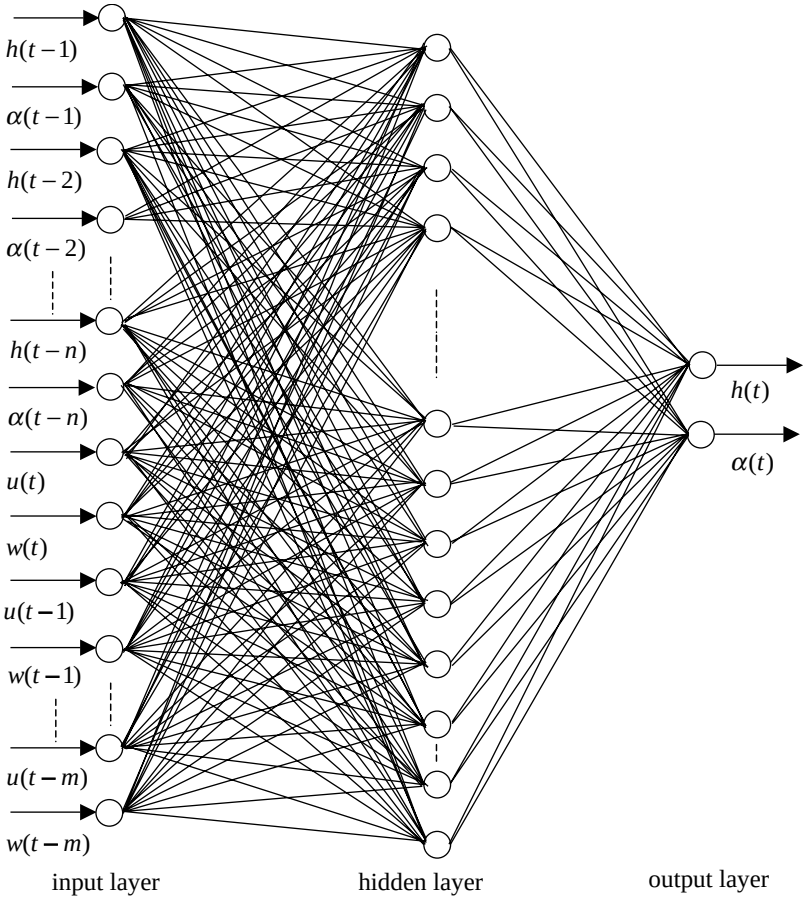

Fig. 3. Three-layer neural network.

where $\{Y\} = (h(t), \alpha(t))^{\mathrm{T}}$, $\{X\} = (\bar{\mathbf{X}}\mathbf{F})^{\mathrm{T}}$,

$$\bar{\mathbf{X}} = (h(t-1)\, a(t-1)\, h(t-2)\, \alpha(t-2) \cdots h(t-n)\, \alpha(t-n)),$$
$$\mathbf{F} = (u(t)\, w(t)\, u(t-1)\, w(t-1) \cdots u(t-m)\, w(t-m)).$$

The elements of $[W]$ and $[V]$ are w_{ij} and v_{ij}, respectively, and the elements of $\{\theta_w\}$ and $\{\theta_v\}$ are θ_{wi} and θ_{vi}. Carefully expanding Eq. (11) yields

$$\begin{Bmatrix} h(t) \\ \alpha(t) \end{Bmatrix} = \sum_{i=1}^{n} \hat{\mathbf{W}}_1^{(i)} \begin{Bmatrix} h(t-i) \\ \alpha(t-i) \end{Bmatrix} + \sum_{j=0}^{m} \hat{\mathbf{W}}_2^{(j)} \begin{Bmatrix} u(t-j) \\ w(t-j) \end{Bmatrix} + \{C\}, \tag{12}$$

where $\lfloor \hat{\mathbf{W}}_1 \;\; \hat{\mathbf{W}}_2 \rfloor = [W][V]$, $\{C\} = [W]\{\theta_v\} + \{\theta_w\}$, $\hat{\mathbf{W}}_1 = [\hat{\mathbf{W}}_1^{(1)} \hat{\mathbf{W}}_1^{(2)} \cdots \hat{\mathbf{W}}_1^{(n)}]$, and $\hat{\mathbf{W}}_2 = [\hat{\mathbf{W}}_2^{(0)} \hat{\mathbf{W}}_2^{(1)} \cdots \hat{\mathbf{W}}_2^{(m)}]$.

The expression of Eq. (12) is similar to the time-series model, ARX. The ARX model equates the equations of motion as given in Eq. (6). Therefore, the dynamic characteristics of the system, described by Eq. (6), can be obtained from the coefficient matrices of AR [17].

The modal parameters can be determined from the eigenvalues and eigenvectors of $[G]$ by following the procedure of Huang [17], and constructing the following matrix:

$$[G] = \begin{bmatrix} 0 & \mathbf{I} & 0 & 0 & 0 \\ 0 & 0 & \mathbf{I} & 0 & 0 \\ \vdots & \vdots & \vdots & \vdots & \vdots \\ 0 & 0 & 0 & 0 & \mathbf{I} \\ \hat{\mathbf{W}}_1^{(n)} & \hat{\mathbf{W}}_1^{(n-1)} & \cdots & \hat{\mathbf{W}}_1^{(2)} & \hat{\mathbf{W}}_1^{(1)} \end{bmatrix}_{2n*2n}. \tag{13}$$

Let λ_k and $\{\psi_k\}$ denote the kth eigenvalue and eigenvector of $[G]$, respectively. The eigenvalue, λ_k, is generally a complex number, and can thus be written as $a_k + ib_k$. The complex conjugates of λ_k and $\{\psi_k\}$ are also an eigenvalue and eigenvector, respectively. The natural frequency and modal damping of the system, as in Eq. (12) are determined by

$$\tilde{\beta}_k = \sqrt{\alpha_k^2 + \beta_k^2}, \tag{14}$$

$$\xi_k = -\alpha_k/\tilde{\beta}_k, \tag{15}$$

where $\tilde{\beta}_k$ is the pseudo-undamped circular natural frequency, ξ_k is the modal damping ratio:

$$\beta_k = \frac{1}{\Delta t}\tan^{-1}\left(\frac{b_k}{a_k}\right), \tag{16}$$

$$\alpha_k = \frac{1}{2\,\Delta t}\ln(a_k^2 + b_k^2) \tag{17}$$

and $1/\Delta t$ is the sampling rate of measurement.

The special composition of $[G]$ in Eq. (13) is such that its eigenvectors exhibit the following property:

$$\{\psi_k\} = (\{\psi_k\}_1^{\mathrm{T}}, \lambda_k\{\psi_k\}_1^{\mathrm{T}}, \lambda_k^2\{\psi_k\}_1^{\mathrm{T}}, \ldots, \lambda_k^{n-1}\{\psi_k\}_1^{\mathrm{T}})^{\mathrm{T}}, \tag{18}$$

where $\{\psi_k\}_1$ is the modal shape of the system that corresponds to the natural frequency, $\tilde{\beta}_k$.

Notably, the number, n, in constructing an ANN is commonly larger than the number of degrees of freedom for the structural system under consideration, to fit appropriately to the measured data. Therefore, the number of eigenvalues of $[G]$ in Eq. (13) is often larger than the number of the natural frequencies for the structural system. It means that, as well as real mechanical modes, extra spurious modes are generated from the constructed ANN. Nevertheless, the eigenvalues and eigenvectors that correspond to real mechanical modes occur consistently as n increases.

λ_k and $\{\psi_k\}_1$ corresponding to real mechanical modes can be easily identified from the observed dynamic responses since Eq. (6) represents a structural system with only two degrees of freedom. Therefore, knowing $\bar{m}$ and $\bar{I}$, enables c_{ij}^{eff} and k_{ij}^{eff} in Eq. (6) to be determined easily. The derivation of Huang [18] shows that $\{\phi_k\} = (\{\psi_k\}_1^{\mathrm{T}}\hat{\lambda}_k\{\psi_k\}_1^{\mathrm{T}})^{\mathrm{T}}$ and $\hat{\lambda}_k$ satisfy

$$\begin{bmatrix} \mathbf{K}^{eff} & \mathbf{0} \\ \mathbf{0} & -\mathbf{M} \end{bmatrix}\{\phi_k\} + \hat{\lambda}_k\begin{bmatrix} \mathbf{C}^{eff} & \mathbf{M} \\ \mathbf{M} & \mathbf{0} \end{bmatrix}\{\phi_k\} = \{0\}, \tag{19}$$

where $\hat{\lambda}_k = \log_e(\lambda_k)/\Delta t$. From the above equation,

$$\begin{bmatrix} \mathbf{C}^{eff} & \mathbf{M} \\ \mathbf{M} & \mathbf{0} \end{bmatrix}^{-1} \begin{bmatrix} \mathbf{K}^{eff} & \mathbf{0} \\ \mathbf{0} & -\mathbf{M} \end{bmatrix} = \mathbf{\Phi}\mathbf{\Lambda}\mathbf{\Phi}^{-1}, \tag{20}$$

where the columns of $\mathbf{\Phi}$ are $\{\phi_k\}$ and its conjugate, and $\mathbf{\Lambda}$ is a diagonal matrix with $\hat{\lambda}_k$ and its conjugate in the diagonal. Expanding Eq. (20) yields

$$\begin{bmatrix} \mathbf{0} & \mathbf{I} \\ -\mathbf{M}^{-1}\mathbf{K}^{eff} & -\mathbf{M}^{-1}\mathbf{C}^{eff} \end{bmatrix} = \mathbf{\Phi}\mathbf{\Lambda}\mathbf{\Phi}^{-1}. \tag{21}$$

From the above equation, $\mathbf{C}^{eff}$ and $\mathbf{K}^{eff}$ can be determined if $\mathbf{M}$ is known.

5. Numerical simulation

Numerical simulations were performed for a section model with two degrees of freedom under flutter force and buffeting force conditions to demonstrate the validity of the proposed identifying procedure. A typical wind tunnel test is usually performed on the section model under smooth flow, while the turbulent flow always affects the measurement for a long cable or suspension bridge.

The scaled stream section model, depicted in Fig. 4 for the Kao Pin Hsi cable-stayed bridge in southern Taiwan, was used in this numerical simulation. This section model is referred to as, "type A". Table 1 lists its material and section properties. The model is assumed to be a mechanically decoupled system with two degrees of freedom, such that the mechanical damping and stiffness matrices in Eq. (1) can be determined from the data given in Table 1. The flutter derivatives of the physical section model, shown in Fig. 5 and denoted as "experimental", were applied to simulate numerically the responses of the system to various wind flow conditions. These flutter derivatives were obtained from wind tunnel tests and are reported in Ref. [19]. Notably, f_v and f_t represent the natural vertical and torsional frequencies of the section model, respectively.

5.1. Flutter force case

The flutter derivatives were determined from the experimental curve shown in Fig. 5 to compute the dynamic responses of the model under smooth flow with a given wind velocity. The effective damping and stiffness matrices corresponding to the given wind velocity were obtained using

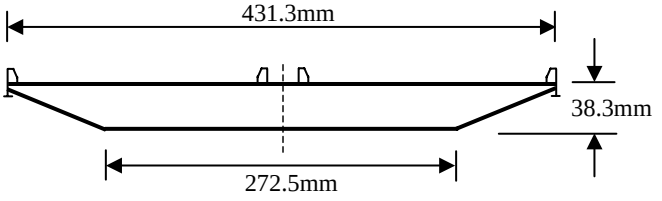

Fig. 4. Cross-section of Kao Ping Hsi bridge model (type A).

Table 1
Model parameters of Kao Ping Hsi bridge (type A)

Item	Unit	Scale
Deck width	m	0.431
Mass	kg/m	4.66
Mass moment of inertia	$kg\,m^2/m$	0.157
Vertical frequency	Hz	2.441
Torsional frequency	Hz	5.591
Vertical damping ratio	%	0.206
Torsional damping ratio	%	0.159

Eq. (7). Then, the dynamic responses were obtained by solving Eq. (6) by direct integration, with no input forces but with a unit initial displacement for each degree of freedom [20]. Figs. 6(a) and (b) show typical vertical and torsional response histories, respectively. The dynamic displacement responses with a duration of 40 s were stored for further analysis. The sampling rate of the data was 50 Hz.

To be consistent with the study cases in the next section, responses from $t = 0$ to 20 s were used to train an ANN. For each wind velocity, an ANN was established. The architecture of the ANN is similar to that shown in Fig. 3 with $n = 8$, and eight nodes in the hidden layer. The effective damping and stiffness matrices in Eq. (6) were estimated using Eq. (21), by constructing $[G]$ in Eq. (13) from the weighting matrices in the ANN, and determining the corresponding eigenvalues and eigenvectors. The flutter derivatives were then determined using Eq. (7). Fig. 5 also presents the obtained flutter derivatives that correspond to various wind flow velocities. These derivatives agree closely with the experimental values. This agreement confirms the feasibility of the proposed procedure in processing dynamic responses under smooth flow, to determine the flutter derivatives.

In addition, the MITD method has been employed to identify the flutter derivatives corresponding to various wind velocities. The results are also depicted in Fig. 5, which shows that these flutter derivatives obtained from the MITD method agree very well with the present values.

5.2. *Buffeting force case*

The buffeting forces due to wind turbulence can be written as quasi-steady expressions, given in Eqs. (4) and (5). The along-wind and vertical components of wind gusts, $u(t)$ and $w(t)$, are often assumed to be stationary random processes and prescribed by their auto-spectral density functions. The auto-spectral density functions suggested by Simiu and Scanlan [21] were used in this simulation:

$$\frac{\omega S_{uu}(\omega)}{u_*^2} = \frac{200f}{(1+50f)^{5/3}}, \tag{22a}$$

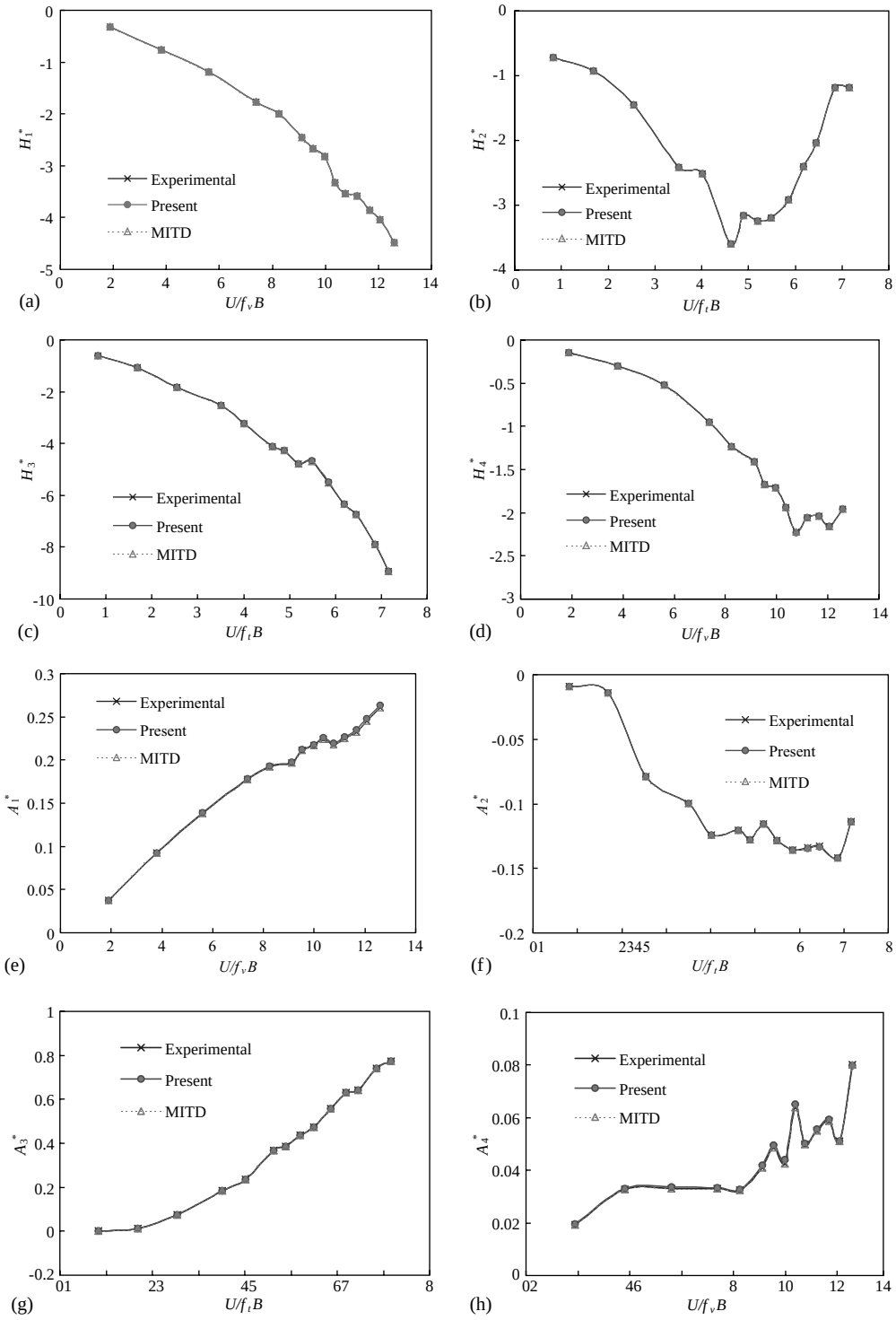

Fig. 5. Comparison of identified flutter derivatives with experiment one for the Kao Ping Hsi bridge section model: (a) H_1^*; (b) H_2^*; (c) H_3^*; (d) H_4^*; (e) A_1^*; (f) A_2^*; (g) A_3^*; (h) A_4^* (flutter force case).

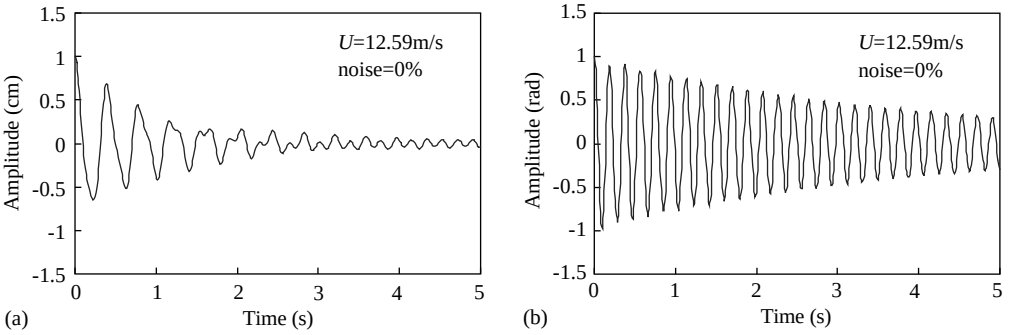

Fig. 6. A set of simulated data under flutter forces: (a) vertical response; (b) torsional response.

$$\frac{\omega S_{ww}(\omega)}{u_*^2} = \frac{3.36f}{(1+10f^{5/3})}, \tag{22b}$$

where S_{uu} and S_{ww} are the auto-spectral density functions of u and w, respectively, $f = \omega z/U(z)$, z is the height of the deck above ground and is set to 50 m, ω is the frequency of the wind, and u_* is the friction velocity which depends on the surface's roughness. The surface roughness is set to 0.3 m such that u_* can be determined from the formulation given in Ref. [21].

Time histories for u and w must be generated to compute the dynamic responses of the section model in the time domain. Accordingly, the procedure of Cao et al. [22] was adopted here. The stochastic wind field was simulated from the corresponding auto-spectral density function by

$$g_j(t) = \sqrt{2(\Delta\omega)} \sum_{k=1}^{j} \sum_{l=1}^{N} \sqrt{S_{kl}(\omega)} G_{jk}(\omega) \cos(\omega_{kl} t + \phi_{kl}), \quad j = 1, 2, \tag{23}$$

where $g_1(t) = u(t), g_2(t) = w(t)$, N is the number of data points, $\Delta\omega$ is the increment in frequency, ϕ_{kl} are the sequences of independent random phase angles, and $S(\omega_{kl})$ is the cross-spectral density matrix, which can be expressed as

$$S_{jk}(\omega) = \sqrt{S_{jj}(\omega) S_{kk}(\omega)}\, Coh(\Delta_{jk}, \omega), \quad j, k = 1, 2 \text{ and } j \neq k, \tag{24}$$

where $Coh(\Delta_{jk}, \omega)$ is the coherence function between j and k, given in Ref. [22]. $G_{jk}(\omega)$ is the coefficient matrix, which is concerned with the complex frequency response and auto-spectral density functions [22]. C_L, C_D, C_M, $\partial C_L/\partial\alpha$, and $\partial C_M/\partial\alpha$ are set equal to -0.39, 0.95, 0.017, 6.1302 rad^{-1}, 1.9551 rad^{-1}, respectively, in determining the buffeting forces. Then, the dynamic responses under turbulent flows of the system with two degrees of freedom can be found using the direct integration scheme used in the previous section. Fig. 7 shows a set of typical, simulated dynamic responses. The displacement response histories were generated with a duration of 40 s. Again, the sampling rate was 50 Hz.

Simulated dynamic displacement responses for the early 20 s, which show the decaying characteristics, are used to train an ANN with the architecture depicted in Fig. 3 for $m = n = 8$ and a hidden layer of 16 nodes. The identified results corresponding to various mean velocities are also shown in Fig. 8 and are denoted as "B-0%". These results are also excellently consistent with the experimental results.

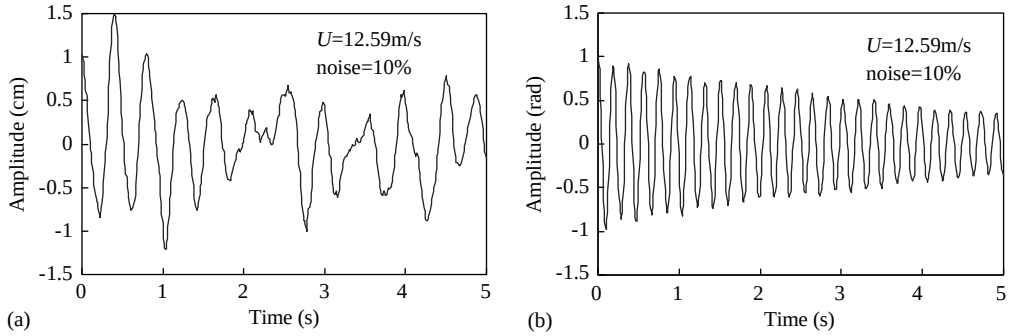

Fig. 7. A set of simulated data under buffeting forces: (a) vertical response; (b) torsional response.

In reality, measured responses always contain some corrupted noise. Noise with 10% variance in the signal-to-noise ratio was randomly added to the simulated responses, to somewhat simulate this situation. These responses were then used to train an ANN with $m = n = 12$ and a hidden layer of 16 nodes. The values of m and n in the input layer must increase to yield accurate results, because of the introduction of the noise. The identified flutter derivatives are also given in Fig. 8 and are denoted as "B-10%". Notably, in training an ANN only the simulated responses for the early 20 s were used to somewhat eliminate the effects of noises on identifying the flutter derivatives. Although the identified results are not as good as those obtained for the case without noise, the identified and experimental results remain highly consistent, ensuring the validity of the proposed method in processing noisy data.

6. Wind tunnel experiment

This work uses measured responses of a sectional model in wind tunnel tests to determine the flutter derivatives of the model under smooth flow. An inverted-U deck section, as illustrated in Fig. 9, was used in wind tunnel tests with smooth flow. The section model is denoted as a "type-B" model in the following, and is similar to an unstable bluff box deck model. The motion of the section model can be described simply with two degrees of freedom—namely, vertical and torsional.

The experiments were performed at the atmospheric boundary layer wind tunnel laboratory of Tamkang University in Taiwan. The atmospheric boundary layer wind tunnel is an open-circuit, low-speed wind tunnel. The total length of the wind tunnel is 29.5 m; the test section is 18.7 m long, 3.2 m wide and 2.0 m high. A turntable (3.0 m in diameter) in the test section can be rotated easily to alter the direction of the wind's flowing to the model. A 175 hp, constant-speed motor driving a 2.1 m diameter, variable-pitch fan gives a maximum wind speed of 18 m/s. The 4:1 contraction section contains honeycombs and four screens to produce low-turbulence flow at the entrance of the test section. Installing both generators of suitable vorticity and surface roughness elements in the test section enables the mean flow and turbulence structure of strong winds to be simulated correctly, at model scales between 1/100 and 1/1000.

Table 2 summarizes the geometrical and material properties of the section model [23]. Fig. 10 plots a set of typical displacement response histories for vertical and torsional motions. The

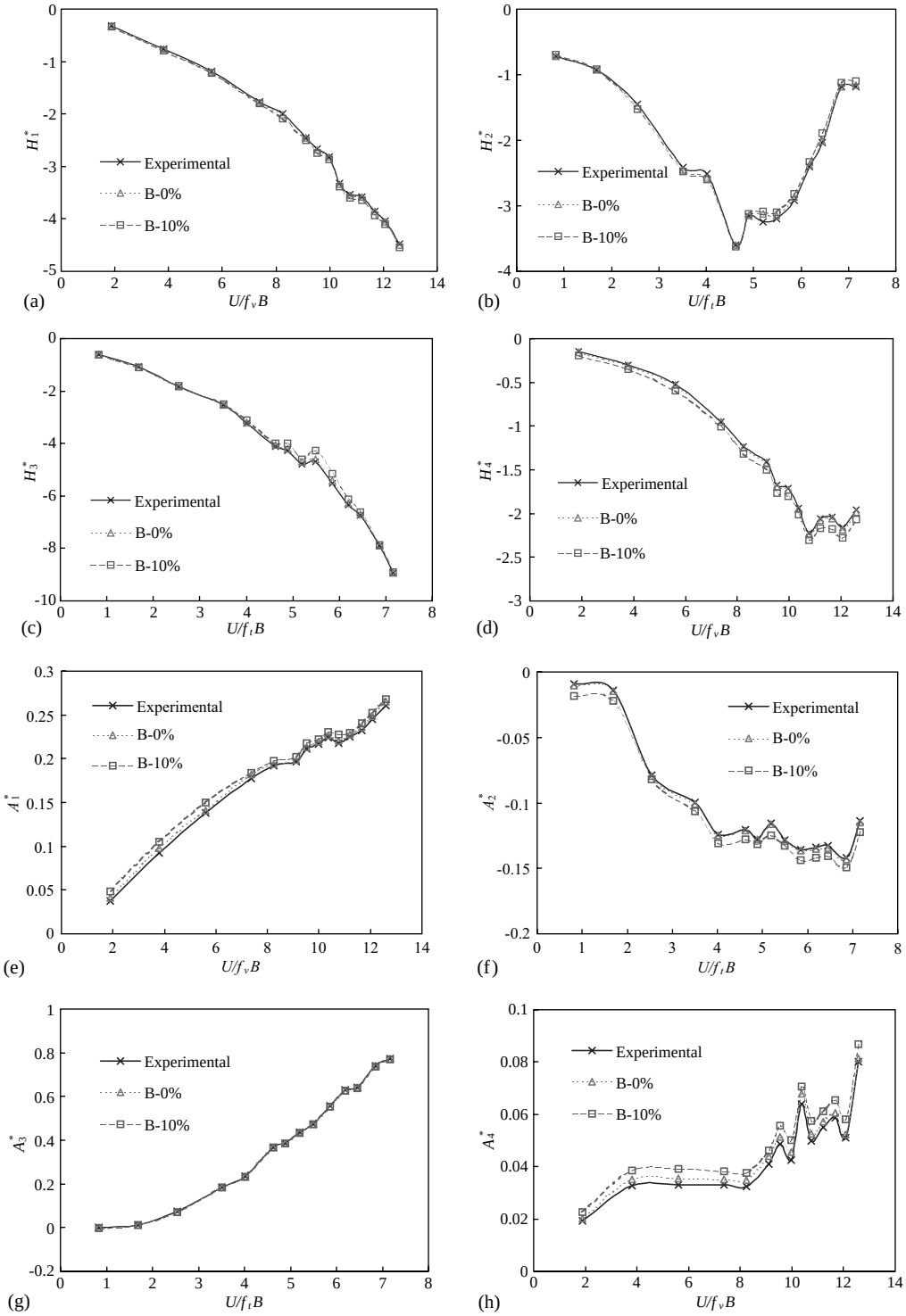

Fig. 8. Comparison of identified flutter derivatives with experiment one for the Kao Ping Hsi bridge section model: (a) H_1^*; (b) H_2^*; (c) H_3^*; (d) H_4^*; (e) A_1^*; (f) A_2^*; (g) A_3^*; (h) A_4^* (buffeting force case).

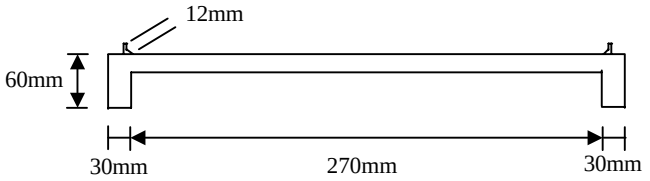

Fig. 9. Cross-section of type B model.

Table 2
Model parameters of section model type B

Item	Unit	Scale
Deck width	m	0.345
Mass	kg/m	2.8707
Mass moment of inertia	$kg\,m^2/m$	25.27×10^{-3}
Vertical frequency	Hz	2.71
Torsional frequency	Hz	6.04
Vertical damping ratio	%	0.779
Torsional damping ratio	%	0.129

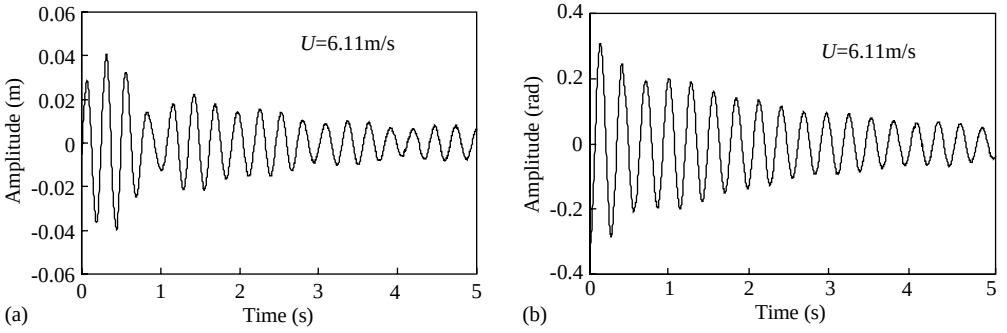

Fig. 10. A typical set of experiment data under smooth flow: (a) vertical response; (b) torsional response.

responses were recorded over 10 s, at a sampling rate of 250 Hz. The present identification procedure was applied to experimental data that corresponded to various mean wind velocities without preprocessing.

Fig. 11 presents the variation of the identified flutter derivatives with the inverse of the dimensionless reduced frequency, $2\pi/K$. The magnitudes of A_3*, H_1*, and H_4* increase with $2\pi/K$, while the other flutter derivatives do not show such a monotonic trend. The fluctuations of these identified flutter derivatives with $2\pi/K$ are similar to those for the unstable bluff box deck model, obtained by Scanlan [13]. Notably, the findings of Scanlan [13] and the trend in Fig. 11(d), suggest that the positive value of A_2* should increase with $2\pi/K$.

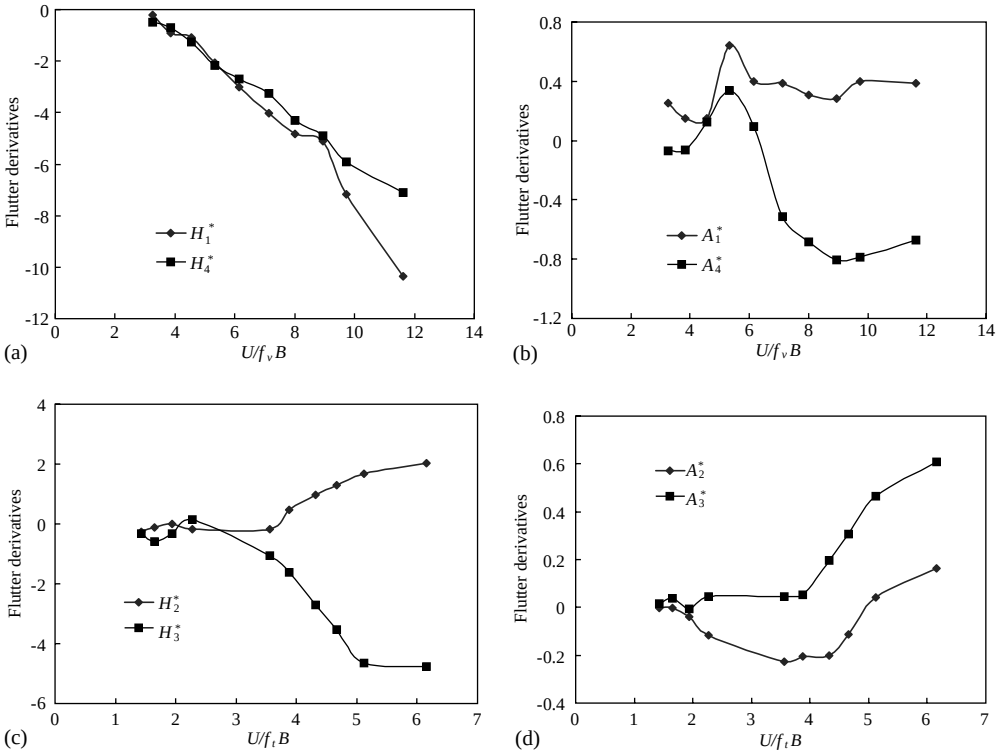

Fig. 11. Flutter derivatives of type B section model: (a) H_1^* and H_4^*; (b) A_1^* and A_4^*; (c) H_2^* and H_3^*; (d) A_2^* and A_3^*.

Cable-supported bridges are usually designed to have the natural frequency of the first torsional mode higher than that of the first vertical mode. The flutter derivatives, H_4* and A_3* are well known greatly to influence the vibration frequencies of vertical and torsional modes, respectively. Eq. (7) reveals that the negative value of H_4* and positive value of A_3*, given in Fig. 11, would result in an increase in the vibration frequency of the vertical mode and a decrease in the vibration frequency of the torsional mode, as wind velocity increases. Therefore, these two vibration frequencies are expected to be the same at a certain wind velocity due to the degeneracy of eigenvalues, and the so-called stiffness-driven flutter instability occurs [24].

The flutter derivatives, H_1* and A_2* were reported to influence significantly the modal damping of vertical and torsional modes, respectively [21]. A negative value of H_1*, whose magnitude increases with wind velocity, results in increased net damping of vertical motion. The negative values of A_2* given in Fig. 11, also result in an increase in the net damping of the torsional mode. However, as mentioned above, positive values of A_2* are expected to increase for a wind velocity that rises far above the range considered in the figure, such that the net damping becomes negative at a certain, high velocity. Then, the so-called damping-driven flutter instability occurs [24]. Comparing the values of A_2* for the type B model (Fig. 11(d)) with those for the type A model (Fig. 5(f)) reveals that the former model more easily suffers damping-driven flutter instability than the latter.

7. Concluding remarks

This study has explored a novel procedure, based on using artificial neural networks, to determine the flutter derivatives of a section model from its dynamic responses under smooth or turbulent flow. The method is based on establishing a high-fidelity neural network to match the observed responses. The modal parameters of the section model for various mean velocities of wind flow are directly estimated from the weighting matrices in the neural network. Then, the flutter derivatives, which depend on mean flow velocity, are obtained through matrix operations on the modal parameters.

Numerical simulations of a section model under smooth and turbulent flows have been performed to confirm the validity of the proposed procedure. The present procedure has been shown to be able to accurately determine the variation of the flutter derivatives with the mean velocity of the wind, even for dynamic responses with corrupting noise.

The present procedure has been applied to real data obtained from wind tunnel tests on an inverted-U-type section model to demonstrate its practicability. The trends in the variations of identified flutter derivatives with $2\pi/K$ are similar to those for the unstable bluff box deck model, obtained by Scanlan [13], due to the similarity of the two section models. The identified flutter derivatives indicate that the stiffness-driven flutter instability and the damping-driven flutter instability can easily occur in this section model.

Acknowledgements

The authors would like to thank the National Science Council of the Republic of China for financially supporting this research under Contract No. NSC_89-2211-E-033-011.

References

[1] R.H. Scanlan, J.J. Tomko, Airfoil and bridge deck flutter derivatives, Journal of Engineering Mechanics Division, American Society of Civil Engineers 97 (6) (1971) 1717–1737.
[2] T. Kumarasena, Wind Response Prediction of Long-span Bridges, Ph.D. Thesis, The Johns Hopkins University, Baltimore, MD, USA, 1989.
[3] M. Shinozuka, C.B. Yun, H. Imai, Identification of linear structural dynamic system, Journal of the Engineering Mechanics Division, American Society of Civil Engineers 108 (6) (1982) 1371–1390.
[4] K. Imai, C.B. Yun, O. Maruyama, M. Shinozuka, Fundamentals of system identification in structural dynamics, Probabilistic Engineering Mechanics 4 (4) (1989) 162–173.
[5] P.P. Sarkar, N.P. Jones, R.H. Scanlan, System identification for estimation of flutter derivatives, Journal of Wind Engineering and Industrial Aerodynamics 41–44 (1992) 1243–1254.
[6] P.P. Sarkar, N.P. Jones, R.H. Scanlan, Identification of aeroelastic parameters of flexible bridges, Journal of Engineering Mechanics, American Society of Civil Engineers 120 (8) (1994) 1718–1742.
[7] N.K. Poulsen, A. Damsgaard, T.A. Reinhold, Determination of flutter derivatives for the Great Belt bridge, Journal of Wind Engineering and Industrial Aerodynamics 41 (1992) 153–164.
[8] H. Yamada, T. Miyata, H. Ichikawa, Measurement of aerodynamic coefficients by system identification methods, Journal of Wind Engineering and Industrial Aerodynamics 41–44 (1992) 1255–1263.
[9] M. Iwamoto, Y. Fujino, Identification of flutter derivatives of bridge deck from free vibration data, Journal of Wind Engineering and Industrial Aerodynamics 54–55 (1995) 55–63.

[10] J. Bogunovic Jakobsen, E. Hjorth-Hansen, Determination of the aerodynamic derivatives by a system identification method, Journal of Wind Engineering and Industrial Aerodynamics 57 (1995) 295–305.
[11] P. Zeng, Neural computing in mechanics, Applied Mechanics Review 51 (2) (1998) 173–197.
[12] R.H. Scanlan, Interpreting aeroelastic models of cable-stayed bridges, Journal of Engineering Mechanics, American Society of Civil Engineers 113 (4) (1987) 555–575.
[13] R.H. Scanlan, The action of flexible bridges under wind, I: flutter theory, Journal of Sound and Vibration 60 (2) (1978) 187–199.
[14] D.E. Rumelnart, G.E. Hinton, R.J. Williams, Learning international representation by error propagation, in: D.E. Rumelnart, et al. (Eds.), Parallel Distributed Processing, The MIT Press, Cambridge, MA, 1986, pp. 318–362.
[15] R. Hecht-Nielsen, Theory of the back propagation neural network, Proceedings of the International Joint Conference on Neural Networks, Vol. 1, IEEE, 1989, pp. 593–605.
[16] M.T. Hagan, M.B. Menhaj, Training feedforward networks with the Marquardt algorithm, IEEE Transactions on Neural Networks 5 (6) (1994) 989–993.
[17] C.S. Huang, Structural identification from ambient vibration measurement using the multivariate AR model, Journal of Sound and Vibration 241 (3) (2001) 337–359.
[18] C.S. Huang, A study on techniques for analyzing ambient vibration measurement (II)—time series methods, Report No. NCREE-99-018, National Center for Research on Earthquake Engineering, ROC, 1999.
[19] Vienna Consulting Engineers, Wind-tunnel tests for Kao Ping Hsi bridge: section model tests, 1993.
[20] R.W. Clough, J. Penzien, Dynamics of Structures, 2nd Edition, McGraw-Hill, New York, 1993.
[21] E. Simiu, R.H. Scanlan, Wind Effects on Structures: Fundamentals and Applications to Design, 3rd Edition, Wiley, New York, 1996.
[22] Y. Cao, H. Xiang, Y. Zhou, Simulation of stochastic wind velocity field on long-span bridges, Journal of Engineering Mechanics, American Society of Civil Engineers 126 (1) (2000) 778–787.
[23] C.L. Huang, The Section Model Tests and Identification of the Flutter Derivatives Applied to Cable-stayed Bridge, Master Thesis, National Taiwan University, Taipei, Taiwan, 2000.
[24] A.H. Namini, Analytical modeling of flutter derivatives as finite elements, Computers and Structures 41 (5) (1991) 1055–1064.